Original Article
Mol Imaging Radionucl Ther 2022;31:82-88 DOI:10.4274/mirt.galenos.2021.43760

Diagnostic Performance of Machine Learning Models Based on ^{18}F-FDG PET/CT Radiomic Features in the Classification of Solitary Pulmonary Nodules

Soliter Pulmoner Nodüllerin Sınıflandırılmasında ^{18}F-FDG PET/BT Radyomik Özelliklerine Dayalı Makine Öğrenme Modellerinin Tanısal Performansı

Yavuz Sami Salihoğlu[1], Rabiye Uslu Erdemir[2], Büşra Aydur Püren[1], Semra Özdemir[1], Çağlar Uyulan[3], Türker Tekin Ergüzel[4], Hüseyin Ozan Tekin[5]

[1]Çanakkale Onsekiz Mart University Faculty of Medicine, Department of Nuclear Medicine, Çanakkale, Turkey
[2]Zonguldak Bülent Ecevit University Faculty of Medicine, Department of Nuclear Medicine, Zonguldak, Turkey
[3]İzmir Katip Çelebi University Faculty of Engineering and Architecture, Department of Mechanical Engineering, İzmir, Turkey
[4]Üsküdar University Faculty of Natural Sciences, Department of Software Engineering, İstanbul, Turkey
[5]University of Sharjah, College of Health Sciences, Department of Medical Diagnostic Imaging, Sharjah, United Arab Emirates

Abstract

Objectives: This study aimed to evaluate the ability of ^{18}fluorine-fluorodeoxyglucose (^{18}F-FDG) positron emission tomography/computed tomography (PET/CT) radiomic features combined with machine learning methods to distinguish between benign and malignant solitary pulmonary nodules (SPN).

Methods: Data of 48 patients with SPN detected on ^{18}F-FDG PET/CT scan were evaluated retrospectively. The texture feature extraction from PET/CT images was performed using an open-source application (LIFEx). Deep learning and classical machine learning algorithms were used to build the models. Final diagnosis was confirmed by pathology and follow-up was accepted as the reference. The performances of the models were assessed by the following metrics: Sensitivity, specificity, accuracy, and area under the receiver operator characteristic curve (AUC).

Results: The predictive models provided reasonable performance for the differential diagnosis of SPNs (AUCs ~0.81). The accuracy and AUC of the radiomic models were similar to the visual interpretation. However, when compared to the conventional evaluation, the sensitivity of the deep learning model (88% vs. 83%) and specificity of the classic learning model were higher (86% vs. 79%).

Conclusion: Machine learning based on ^{18}F-FDG PET/CT texture features can contribute to the conventional evaluation to distinguish between benign and malignant lung nodules.

Keywords: Solitary pulmonary nodule, PET/CT, radiomic, machine learning

Öz

Amaç: Bu çalışmada, ^{18}flor-florodeoksiglukoz (^{18}F-FDG) pozitron emisyon tomografisi/bilgisayarlı tomografi (PET/BT) radyomik özelliklerinin makine öğrenme yöntemleriyle birleştirilmesinin benign ve malign soliter pulmoner nodülleri (SPN) ayırt etme yeteneğini değerlendirmeyi amaçladık.

Yöntem: ^{18}F-FDG PET/BT taramasında SPN saptanan 48 hastanın verileri geriye dönük olarak değerlendirildi. PET/BT görüntülerinden doku özelliği çıkarımı, açık kaynaklı bir uygulama (LIFEx) kullanılarak yapıldı. Modelleri oluşturmak için derin öğrenme ve klasik makine öğrenme algoritmaları

Address for Correspondence: Yavuz Sami Salihoğlu Asst. Prof., Çanakkale Onsekiz Mart University Faculty of Medicine, Department of Nuclear Medicine, Çanakkale, Turkey
Phone: +90 286 263 59 50-2034 **E-mail:** yssalihoglu@hotmail.com ORCID ID: orcid.org/0000-0003-2465-9128
Received: 03.09.2021 **Accepted:** 26.12.2021

©Copyright 2022 by Turkish Society of Nuclear Medicine
Molecular Imaging and Radionuclide Therapy published by Galenos Yayınevi.

kullanıldı. Patoloji ve izlem ile kesinleşen tanı referans olarak kabul edildi. Modellerin performansları şu metriklerle değerlendirildi: Duyarlılık, özgüllük, doğruluk ve alıcı operatör özellikleri eğrisi altındaki alan (EAA).

Bulgular: Tahmine dayalı modeller, SPN'lerin ayırıcı tanısı için makul performans sağlandı (EAA'ler ~0,81). Radyomik modellerin doğruluğu ve EAA'sı görsel yorumlamaya benzerdi. Ancak geleneksel değerlendirme ile karşılaştırıldığında, derin öğrenme modelinin duyarlılığı (%88'e karşı %83) ve klasik öğrenme modelinin özgüllüğü (%86'ya karşı %79) daha yüksekti.

Sonuç: ^{18}F-FDG PET/BT doku özelliklerine dayalı makine öğrenimi, iyi huylu ve kötü huylu akciğer nodüllerini ayırt etmek için geleneksel değerlendirmeye katkıda bulunabilir.

Anahtar kelimeler: Soliter pulmoner nodül, PET/BT, radyomik, makine öğrenmesi

Introduction

Lung cancer is an important health problem, representing about a quarter of all cancers (1). Early-stage lung cancer may manifest as pulmonary nodules with several distinct features on medical imaging. A solitary pulmonary nodule (SPN) is defined as a well-marginated, rounded parenchymal lesion less than 30 mm in diameter, not associated with other lung pathologies. Common causes of SPN include benign diseases such as infectious granulomas and hamartomas, as well as primary or metastatic lung cancers (2). The management of patients with SPN includes periodic follow-up or further imaging and histopathological examination, considering the malignancy risk (3,4). Positron emission tomography/computed tomography (PET/CT) are widely preferred imaging techniques to detect and characterize SPN, however their diagnostic efficacy does not fully meet clinical needs (5,6).

Radiomics is defined as obtaining high-throughput quantitative features and information from medical images and is a promising approach that has received widespread attention recently (7,8,9,10). Previously, classical machine learning methods and more recently, artificial intelligence applications have been explored for a wide variety of potential uses in lung cancer imaging (11,12,13). Deep learning algorithms using large datasets, such as those from lung cancer screening trials, detect and classify pulmonary nodules with high diagnostic accuracy (13,14).

Several predictive models with generally high diagnostic accuracy based on a combination of radiomic features from lung CT and PET/CT have been proposed for different clinical goals (15,16,17,18,19). Preliminary evidence from these studies is promising however more research is needed to verify these results before clinical application. In this study, we aimed to develop predictive models based on ^{18}fluorine-fluorodeoxyglucose (^{18}F-FDG) PET/CT texture features for the differential diagnosis of SPN and to evaluate the diagnostic performance of these models.

Materials and Methods

Study Populations

The data of patients who underwent ^{18}F-FDG PET/CT between January 2014 and December 2018 were analyzed retrospectively. The patients included had all the criteria following: (i) ^{18}F-FDG avid SPN detected on PET/CT (n=108); (ii) availability of pathological evidence or at least one-year follow-up (n=80) for the final diagnosis of nodules, as a reference standard. The exclusion criteria are as follows: (i) Nodules at the base of the lungs likely to cause respiratory artifacts (n=15); (ii) nodules with too small metabolic volume to allow adequate tissue features to be extracted (n=17). Finally, the data of 48 patients were evaluated under the above criteria. The Local Ethics Committee of Canakkale Onsekiz Mart University Faculty of Medicine approved this study under the decision number: 09.12.2020/2020-14 and patient informed consent was waived.

PET/CT Acquisition Procedure

^{18}F-FDG PET/CT scans were performed using an integrated PET/CT system (Gemini TF16 PET/CT; Philips Medical Systems). PET images were acquired 60±5 minutes after the intravenous injection of ^{18}F-FDG at a dose of 350-550 MBq in patients who fasted for at least 6 hours and had blood glucose <150 mg/dL. First, a low-dose CT scan (120 kVp peak voltage, of 60-150 mA automated tube current, and 5 mm slice thickness) without contrast enhancement was acquired from the skull vertex to the proximal thigh. Then, PET images were acquired for 2-3 minutes per bed position in 3D mode. PET images were reconstructed using the line-of-response row-action maximum likelihood algorithm (LOR-RAMLA; Philips Astonish TF).

PET/CT Image Interpretation

The PET images were reviewed by two experienced nuclear medicine specialists blinded by the final diagnosis, and the final decision was reached by consensus. The decision for benign and malignant nodules was based on ^{18}F-FDG avidity on PET, along with CT features such as size, margin, density, and calcification (20).

Feature Extraction

An open-source application (LIFEx version 6.30) was used for texture analysis from PET/CT images (21). This application declares Image Biomarker Standardization Initiative compliance. A fixed relative thresholding technique was applied for the tumor delineation on images. A 3-D spherical volume of interest (VOI) was initially placed on the entire lesion. A 40% maximum standardized uptake value (SUV_{max}) threshold was applied to (semi)automatically delineation the VOI of the target lesion on the PET images. All volumes were spatially resampled of 4×4×4 mm in size; absolute resampling was used for intensity rescaling with bounds from 0 to 20 SUV (64 bins, 0.32 fixed bin width); and 64 gray levels were applied for intensity discretization. Radiomic features derived from PET images included conventional indices; first-order features-histogram; shape features; second-order texture features [gray-level co-occurrence matrix (GLCM), gray-level run-length matrix (GLRLM), gray-level zone length matrix (GLZLM) and neighborhood gray-tone different matrix (NGLDM)]. A detailed description of the texture parameters can be found at http://www.lifexsoft.org.

Model Establishment

First, feature selection and dimensionality reduction were applied to the feature dataset using the recursive feature elimination (RFE) method. The RFE is a feature selection method that fits a model and removes the weakest features until the specified number of features is reached (22). We build two prediction models based on supervised machine learning classification algorithms selected feature sets: Extreme gradient boosting (XGB) and deep neural network (DNN) to distinguish between benign and malignant nodules. XGB is a tree-based algorithm under the supervised branch of machine learning. XGB, which ensembles the decision tree methods, uses a computationally efficient descent algorithm to minimize errors while adding new trees (19). Deep learning is multi-layer feed-forward neural network that accepts images as input and can be trained end-to-end in a supervised method while learning highly discriminative image features. The opportunity to use large databases has paved the way for the wider adoption of machine/deep learning techniques, particularly in lung cancer assessment (14).

For all models, the dataset was randomly split into two sets using 70% of the samples for training/validating the models and the remaining 30% for testing the results. The models were evaluated using k-fold cross-validation, with three repeats and 10 folds. Figure 1 illustrates the workflow of the radiomic analysis.

Statistical Analysis

We used IBM SPSS statistics software (version 23.0; SPSS Inc.) and Python software to perform statistical analyses. We investigated the performance of predictive models and compared them with the visual evaluation. The following metrics obtained through the confusion matrix were used to compare the performance of the models: Sensitivity, specificity, accuracy, and area under the receiver operator characteristic curve.

Results

In total, the records of 80 patients with SPN were reviewed. Thirty-two patients were excluded under the exclusion criteria. As a result, the study group consisted of 48 patients (31 males, 17 females) with a mean age of 62.38±11.27 years. All of the malignant nodules and 12 of the benign lesions were pathologically proven; the diagnosis of benign lesions was confirmed by follow-up in 5 patients. Thirty-one lesions were malignant nodules, and 17 lesions were benign. The most common malignant diagnosis was adenocarcinoma (58%), while the benign disease was a granulomatous change (53%). The diagnosis and subtypes of SPNs are summarized in Table 1. The majority of malignant nodules (71%) occurred in the upper lobes, whereas about half of the benign nodules (48%) occurred in the lower lobes. Central calcification was observed in four of the benign nodules and punctual calcification was observed in one of the malignant nodules. While most benign nodules tend to have well-defined edges, about half of the malignant nodules have irregular and poorly defined margins. The average diameter of malignant nodules was 20.32 mm (range 16.1-30) and that of benign nodules was 16.9 mm (range 14.2-30). The average SUV_{max} of malignant nodules was 5.46 (range 1.88-10.33) and that of benign nodules was 2.06 (range 1.12-6.77). While SUV_{max} was <2.5 in 24% (4/17) of malignant nodules, SUV_{max} was >2.5 in 23% (7/31) of benign nodules.

The ten most relevant PET features obtained after feature selection and used to develop predictive models are represented in Table 2. The three features with the highest score by the assessment of feature importance were GLZLM_SZLGE (n=30), HISTO_Energy (n=21), and SUV_{bwmean} (n=21). A few of the second-order features (D_HISTO_Energy, GLCM_Homogeneity, NGLDM_Busyness) were higher in benign nodules, while conventional SUV-related features and other second-order features were higher in the malignant group. Texture features that differ significantly between malignant and benign nodules are shown in Table 3.

Table 4 shows the performance of radiomic models and visual interpretation in the differential diagnosis of SPN.

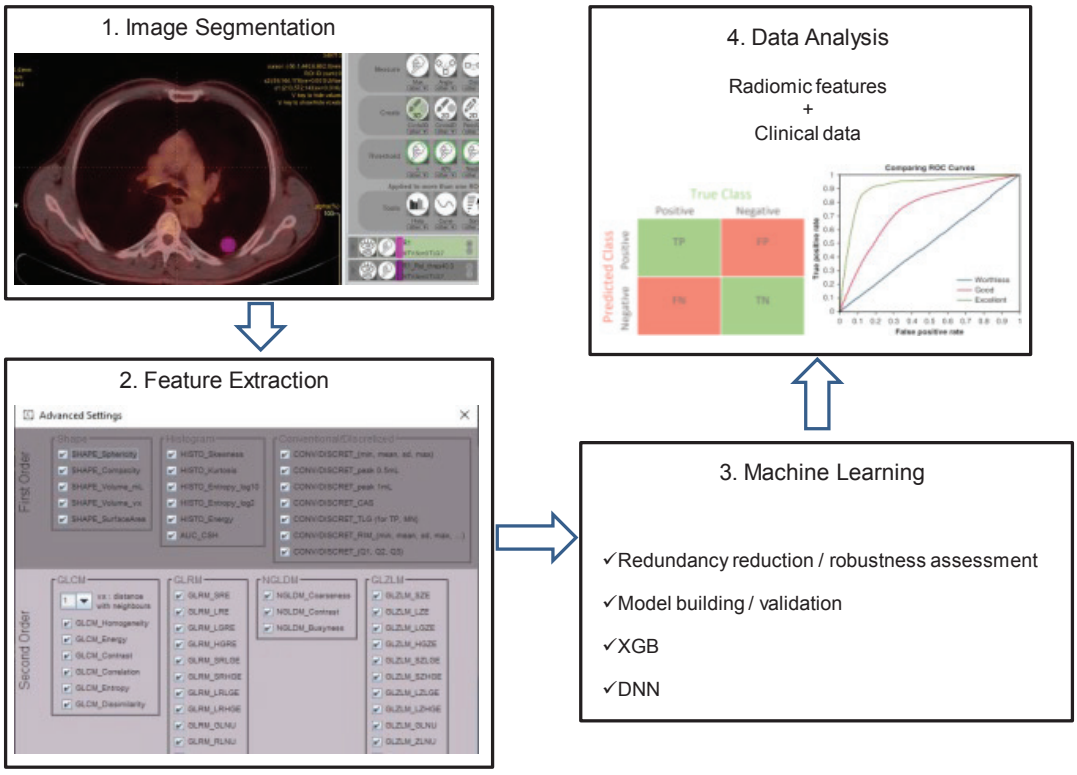


Figure 1. The flowchart of radiomics. 1) The VOI was (semi)automatically defined on PET/CT images with a threshold of 40% of the SUV_{max}. 2) Radiomic features from the VOI were extracted, including first-order and second-order features. 3) Predictive models were established by feature selection methods and classification methods. 4) The model's performance was evaluated by appropriate statistical methods
VOI: Volume of interest, PET/CT: Positron emission tomography/computed tomography, SUV_{max}: Maximum standardized uptake value

Table 1. The diagnosis and subtypes of the SPNs

Type	Diagnosis	Number
Benign (n=17)	Infectious granuloma	9
	Hamartoma	3
	Not specified*	5
Malignant (n=31)	Adenocarcinoma	18
	Squamous cell carcinoma	7
	Metastasis	2
	Small cell carcinoma	2
	Carcinoid tumor	2

*Diagnosed by follow-up, SPNs: Solitary pulmonary nodules

Table 2. The most relevant PET features obtained after feature selection

f score	Texture features
f0	C_SUV_{bwmean}
f1	D_HISTO_Energy
f2	GLCM_Energy
f3	GLCM_Dissimilarity
f4	GLRLM_HGRE
f5	GLRLM_SRHGE
f6	GLRLM_LRHGE
f7	NGLDM_Busyness
f8	GLZLM_SZLGE
f9	GLZLM_SZHGE

SUV: Standardized uptake value, GLCM: Gray-level co-occurrence matrix, GLRLM: Gray-level run-length matrix, NGLDM: Neighborhood gray-tone different matrix, GLZLM: Gray-level zone length matrix

The overall diagnostic performances of both models were close to each other. The DNN model improved sensitivity, while the XGB model increased specificity compared to visual assessment.

Discussion

In this study, we evaluated the performance of machine learning models based on ^{18}F-FDG PET/CT radiomic features for SPN classification. We have shown that the diagnostic accuracy of predictive models is higher than that of commonly used clinical metrics and visual interpretation. The improved diagnostic performance could benefit by

Table 3. Texture features with significant differences between malignant benign nodules

Features	Benign SPN	Malign SPN	p
C_SUV$_{bwmin}$	1.19±0.75	2.61±1.27	0.0003
C_SUV$_{bwmean}$	2.52±1.63	6.53±2.62	<0.0001
C_SUV$_{bwmax}$	4.11±2.56	10.85±4.52	<0.0001
D_HISTO_Energy	0.22±0.14	0.08±0.03	<0.0001
GLCM_Homogeneity	0.54±0.17	0.33±0.11	<0.0001
GLCM_Energy	0.081±0.19	0.014±0.011	<0.0001
GLCM_Dissimilarity	1.27±1.21	4.72±2.13	<0.0001
GLRLM_HGRE	124±104	567±232	<0.0001
GLRLM_SRHGE	95±121	543±423	<0.0001
GLRLM_LRHGE	148.95±137.49	672.55±470.7	<0.0001
NGLDM_Busyness	0.87±0.52	0.24±0.23	<0.0001
GLZLM_SZLGE	0.013±0.013	0.004±0.008	<0.0001
GLZLM_SZHGE	48.75±45.77	342.91±306.06	<0.0001

SPN: Solitary pulmonary nodule, SUV: Standardized uptake value, GLCM: Gray-level co-occurrence matrix, GLRLM: Gray-level run-length matrix, NGLDM: Neighborhood gray-tone different matrix, GLZLM: Gray-level zone length matrix

Table 4. The estimated performances of radiomic models and visual interpretation

Model	SN	SP	ACC	AUC
DNN	88%	82%	0.80	0.81
XGB	81%	86%	0.79	0.80
VI	83%	79%	0.80	0.80

SN: Sensitivity, SP: Specificity, ACC: Accuracy, AUC: Area under the curve, DNN: Deep neural network, XGB: Extreme gradient boosting, VI: Visual interpretation

preventing unnecessary invasive tests following false-positive findings or providing an earlier diagnosis of malignant disease.

^{18}F-FDG PET/CT has reasonable sensitivity to differentiate benign from malignant pulmonary nodules but has lower specificity due to granulomatous diseases (5,6,23,24). Many recent studies have concluded that medical image radiomic features improve clinical or imaging outcomes in many cancers. Although the results available in the literature are promising, they have not yet been sufficiently introduced into clinical practice due to well-known limitations such as the lack of use of standardized methods in the workflow and the lack of external validation (9,10,13).

PET/CT radiomics in lung cancer have been investigated for clinical goals such as characterization of nodules, histological subtyping, prediction of survival, and response to therapy (11,12). Few studies that focused on the characterization of pulmonary nodules demonstrated the ability of PET/CT radiography to distinguish between malign and benign lesions (15,16,17,18,19,25,26,27). In the studies, the results of machine learning models trained with texture features derived from ^{18}F-FDG PET/CT were compared with standard metrics [SUV, metabolic tumor volume (MTV), and total lesion glycolysis] and/or visual interpretation evaluation. Studies with dual time point ^{18}F-FDG PET/CT, particularly the results obtained with tissue properties in delayed images, provided important improvements for classifying SPNs (14,15,27,28). Texture features that reflect intra-lesional heterogeneity, termed second-order texture features in this study, showed significant differences between the malignant and benign groups, as reported in studies.

Our predictive models showed reasonable diagnostic performance with balanced sensitivity and specificity for the differential diagnosis of SPNs. Compared with the conventional evaluation results, the deep learning model increased sensitivity, while the classic machine learning model increased specificity. The overall performance of our models was consistent with the results of the cited studies; however, the improvement in diagnostic accuracy was less than the reported results (15,16,17,18,19). This difference may be due to the small size of our cohort and the fact that the diagnosis of all nodules was not confirmed by pathology. Additionally, most investigators created models with tissue features from dual time-point PET/CT, and higher diagnostic accuracy was reported, particularly from delayed images.

In standard PET/CT scans, respiratory motion adversely affects both alignment and image sharpness, resulting in reduced tracer uptake and an overestimation of MTV (29). Several PET/CT radiomics articles have reported that respiratory motion significantly affects the values of texture features of lung lesions (30,31). These effects differ according to the location of the lesion in the lung; for example, it is more prominent in the lower lobes. Therefore, nodules located in the lower lobes of the lungs were excluded from the radiomic analysis in our study.

It is difficult to compare the results of machine learning studies reported on PET/CT imaging of lung cancer, as researchers have chosen different materials and methods to construct their models. We performed PET/CT radiomic analysis with two models based on classifiers and feature selection methods to improve the quality score of our study, as suggested by Lambin et al. (32). Zhou et al. (19) compared the performance of machine learning models based on PET/CT radiomics for the classification of lung lesions (16). They reported that most classifiers combined with appropriate feature selection methods showed excellent discrimination. They suggested that gradient

boosting decision tree and random forest are the best classification methods. In another study, the deep learning method was compared with classical machine learning methods to classify mediastinal lymph node metastasis in PET/CT images (33). The authors reported that there was no significant difference between the results of deep learning and classical methods, however, machine learning methods have higher sensitivity but lower specificity than doctors.

Study Limitations

Several limitations should be considered in our study. First, this study was a retrospective analysis and inherent selection bias existed. Secondly, the small size of our study population may have adversely affected the performance of machine learning algorithms. Thirdly, the study's lack of external validation limits the generalizability of our results.

Conclusion

In this study, we performed a machine learning-based analysis of pulmonary nodules using PET/CT images. We found that ^{18}F-PET/CT-based radiomic features can provide added value in differentiating SPNs. The method should be further confirmed in large-scale multicenter, ideally prospective studies so that it can be applied in routine clinical practice.

Ethics

Ethics Committee Approval: The Local Ethics Committee of Canakkale Onsekiz Mart University Faculty of Medicine approved this study under the decision number: 09.12.2020/2020-14.

Informed Consent: Patient informed consent was waived.

Peer-review: Externally peer-reviewed.

Authorship Contributions

Design: Y.S.S., Data Collection or Processing: R.U.E., B.A.P., Y.S.S., Ç.U., T.T.E., H.O.T., Analysis or Interpretation: Y.S.S., S.Ö., R.U.E., Literature Search: Y.S.S., R.U.E., Writing: Y.S.S., S.Ö.

Conflict of interest: No conflict of interest was declared by the authors.

Financial Disclosure: The authors declare that this study has received no financial support.

References

1. Siegel RL, Miller KD, Jemal A. Cancer statistics, 2019. CA Cancer J Clin 2019;69:7-34.
2. Nasim F, Ost DE. Management of the solitary pulmonary nodule. Curr Opin Pulm Med 2019;25:344-353.
3. Bai C, Choi CM, Chu CM, Anantham D, Chung-Man Ho J, Khan AZ, Lee JM, Li SY, Saenghirunvattana S, Yim A. Evaluation of pulmonary nodules: clinical practice consensus guidelines for Asia. Chest 2016;150:877-893.
4. MacMahon H, Naidich DP, Goo JM, Lee KS, Leung ANC, Mayo JR, Mehta AC, Ohno Y, Powell CA, Prokop M, Rubin GD, Schaefer-Prokop CM, Travis WD, Van Schil PE, Bankier AA. Guidelines for management of incidental pulmonary nodules detected on CT images: from the Fleischner Society 2017. Radiology 2017;284:228-243.
5. Jia Y, Gong W, Zhang Z, Tu G, Li J, Xiong F, Hou H, Zhang Y, Wu M, Zhang L. Comparing the diagnostic value of ^{18}F-FDG-PET/CT versus CT for differentiating benign and malignant solitary pulmonary nodules: a meta-analysis. J Thorac Dis 2019;11:2082-2098.
6. Divisi D, Barone M, Bertolaccini L, Zaccagna G, Gabriele F, Crisci R. Diagnostic performance of fluorine-18 fluorodeoxyglucose positron emission tomography in the management of solitary pulmonary nodule: a meta-analysis. J Thorac Dis 2018;10(Suppl 7):S779-S789.
7. Zwanenburg A. Radiomics in nuclear medicine: robustness, reproducibility, standardization, and how to avoid data analysis traps and replication crisis. Eur J Nucl Med Mol Imaging 2019;46:2638-2655.
8. Mayerhoefer ME, Materka A, Langs G, Häggström I, Szczypi ski P, Gibbs P, Cook G. Introduction to Radiomics. J Nucl Med 2020;61:488-495.
9. Hatt M, Cheze Le Rest C, Antonorsi N, Tixier F, Tankyevych O, Jaouen V, Lucia F, Bourbonne V, Schick U, Badic B, Visvikis D. Radiomics in PET/CT: current status and future AI-based evolutions. Semin Nucl Med 2021;51:126-133.
10. Piñeiro-Fiel M, Moscoso A, Pubul V, Ruibal Á, Silva-Rodríguez J, Aguiar P. A Systematic review of pet textural analysis and radiomics in cancer. Diagnostics (Basel) 2021;11:380.
11. Bianconi F, Palumbo I, Spanu A, Nuvoli S, Fravolini ML, Palumbo B. PET/CT radiomics in lung cancer: an overview. Appl Sci 2020;10:1718.
12. Manafi-Farid R, Karamzade-Ziarati N, Vali R, Mottaghy FM, Beheshti M. 2-[(18)F]FDG PET/CT radiomics in lung cancer: an overview of the technical aspect and its emerging role in management of the disease. Methods 2021;188:84-97.
13. Krarup MMK, Krokos G, Subesinghe M, Nair A, Fischer BM. Artificial intelligence for the characterization of pulmonary nodules, lung tumors and mediastinal nodes on PET/CT. Semin Nucl Med 2021;51:143-156.
14. Avanzo M, Stancanello J, Pirrone G, Sartor G. Radiomics and deep learning in lung cancer. Strahlenther Onkol 2020;196:879-887.
15. Chen S, Harmon S, Perk T, Li X, Chen M, Li Y, Jeraj R. Diagnostic classification of solitary pulmonary nodules using dual time ^{18}F-FDG PET/CT image texture features in granuloma-endemic regions. Sci Rep 2017;7:9370.
16. Chen S, Harmon S, Perk T, Li X, Chen M, Li Y, Jeraj R. Using neighborhood gray tone difference matrix texture features on dual time point PET/CT images to differentiate malignant from benign FDG-avid solitary pulmonary nodules. Cancer Imaging 2019;19:56.
17. Zhang J, Ma G, Cheng J, Song S, Zhang Y, Shi LQ. Diagnostic classification of solitary pulmonary nodules using support vector machine model based on 2-[18F]fluoro-2-deoxy-D-glucose PET/computed tomography texture features. Nucl Med Commun 2020;41:560-566.
18. Palumbo B, Bianconi F, Palumbo I, Fravolini ML, Minestrini M, Nuvoli S, Stazza ML, Rondini M, Spanu A. Value of shape and texture features from ^{18}F-FDG PET/CT to discriminate between benign and malignant solitary pulmonary nodules: an experimental evaluation. Diagnostics (Basel) 2020;10:696.
19. Zhou Y, Ma XL, Zhang T, Wang J, Zhang T, Tian R. Use of radiomics based on ^{18}F-FDG PET/CT and machine learning methods to aid clinical decision-making in the classification of solitary pulmonary lesions: an innovative approach. Eur J Nucl Med Mol Imaging 2021;48:2904-2913.
20. Cruickshank A, Stieler G, Ameer F. Evaluation of the solitary pulmonary nodule. Intern Med J 2019;49:306-315.

21. Nioche C, Orlhac F, Boughdad S, Reuzé S, Goya-Outi J, Robert C, Pellot-Barakat C, Soussan M, Frouin F, Buvat I. LIFEx: a freeware for radiomic feature calculation in multimodality imaging to accelerate advances in the characterization of tumor heterogeneity. Cancer Res 2018;78:4786-4789.
22. Jeon H, Oh S. Hybrid-recursive feature elimination for efficient feature selection. Applied Sciences 2020;10:3211.
23. Taralli S, Scolozzi V, Foti M, Ricciardi S, Forcione AR, Cardillo G, Calcagni ML. ^{18}F-FDG PET/CT diagnostic performance in solitary and multiple pulmonary nodules detected in patients with previous cancer history: reports of 182 nodules. Eur J Nucl Med Mol Imaging 2019;46:429-436.
24. Deppen SA, Blume JD, Kensinger CD, Morgan AM, Aldrich MC, Massion PP, Walker RC, McPheeters ML, Putnam JB Jr, Grogan EL. Accuracy of FDG-PET to diagnose lung cancer in areas with infectious lung disease: a meta-analysis. JAMA 2014;312:1227-1236.
25. Du D, Gu J, Chen X, Lv W, Feng Q, Rahmim A, Wu H, Lu L. Integration of PET/CT radiomics and semantic features for differentiation between active pulmonary tuberculosis and lung cancer. Mol Imaging Biol 2021;23:287-298.
26. Hu Y, Zhao X, Zhang J, Han J, Dai M. Value of ^{18}F-FDG PET/CT radiomic features to distinguish solitary lung adenocarcinoma from tuberculosis. Eur J Nucl Med Mol Imaging 2021;48:231-240.
27. Nakajo M, Jinguji M, Aoki M, Tani A, Sato M, Yoshiura T. The clinical value of texture analysis of dual-time-point ^{18}F-FDG-PET/CT imaging to differentiate between 18F-FDG-avid benign and malignant pulmonary lesions. Eur Radiol 2020;30:1759-1769.
28. Teramoto A, Tsujimoto M, Inoue T, Tsukamoto T, Imaizumi K, Toyama H, Saito K, Fujita H. Automated classification of pulmonary nodules through a retrospective analysis of conventional CT and two-phase PET images in patients undergoing biopsy. Asia Ocean J Nucl Med Biol 2019;7:29-37.
29. Vaidya M, Creach KM, Frye J, Dehdashti F, Bradley JD, El Naqa I. Combined PET/CT image characteristics for radiotherapy tumor response in lung cancer. Radiother Oncol 2012;102:239-245.
30. Oliver JA, Budzevich M, Zhang GG, Dilling TJ, Latifi K, Moros EG. Variability of image features computed from conventional and respiratory-gated PET/CT images of lung cancer. Transl Oncol 2015;8:524-534.
31. Grootjans W, Tixier F, van der Vos CS, Vriens D, Le Rest CC, Bussink J, Oyen WJ, de Geus-Oei LF, Visvikis D, Visser EP. The Impact of optimal respiratory gating and image noise on evaluation of intratumor heterogeneity on 18F-FDG PET imaging of lung cancer. J Nucl Med 2016;57:1692-1698.
32. Lambin P, Leijenaar RTH, Deist TM, Peerlings J, de Jong EEC, van Timmeren J, Sanduleanu S, Larue RTHM, Even AJG, Jochems A, van Wijk Y, Woodruff H, van Soest J, Lustberg T, Roelofs E, van Elmpt W, Dekker A, Mottaghy FM, Wildberger JE, Walsh S. Radiomics: the bridge between medical imaging and personalized medicine. Nat Rev Clin Oncol 2017;14:749-762.
33. Wang H, Zhou Z, Li Y, Chen Z, Lu P, Wang W, Liu W, Yu L. Comparison of machine learning methods for classifying mediastinal lymph node metastasis of non-small cell lung cancer from ^{18}F-FDG PET/CT images. EJNMMI Res 2017;7:11.